Fiber In-Line Michelson Interferometer Tip Sensor Fabricated by Femtosecond Laser

Changrui R. Liao, D. N. Wang, *Senior Member, IEEE*, Min Wang, and Minghong Yang

***Abstract*— A fiber in-line Michelson interferometer tip sensor based on open micro-cavity, which is fabricated by femtosecond laser micromachining and the thin film coating technique, is proposed and demonstrated. When used in refractive index sensing, such an interferometer operates in a reflection mode of detection, and exhibits a compact sensor head, good mechanical reliability, wide operation range, and high sensitivity of 975 nm/refractive index unit at a refractive index value of 1.484.**

***Index Terms*— Femtosecond laser, fiber sensor, Michelson interferometer.**

I. Introduction

FIBER in-line interferometers have attracted considerable research interests in recent years because of their compactness, ease of construction and convenient operation in many sensing applications. Various types of fiber in-line interferometer configurations have been demonstrated such as Fabry–Pérot interferometers (FPIs) and Mach–Zehnder interferometers (MZIs) based on thin-film mirrors [1], air bubble [2], long period gratings [3], tapers [4], mismatched fiber cores [5], selective infiltrated photonic crystal fiber (PCF) [6] and open micro-cavity [7]–[9]. The open micro-cavity based interferometers are especially attractive for refractive index (RI) sensing owing to their high sensitivity, ultra-compact sensor head, small temperature cross-sensitivity and flexible tuning of sensitivity and operating range.

In this letter, we demonstrate a compact fiber in-line Michelson interferometer (MI) tip sensor based on open micro-cavity, fabricated by femtosecond (fs) laser micromachining and thin-film coating. The MI consists of a section of single mode fiber (SMF), with partially removed fiber core near one fiber end. The light propagating in the fiber core is along two paths: one is reflected by the cut end of the removed core and the other traveling along the remaining core is reflected back by the fiber end, thus forming two arms of an MI. Ag thin-film is deposited on both the cut end of the core and the fiber end to enhance the reflectivity. Such an MI operates in a reflection mode of detection, exhibits high sensitivity and wide sensing range.

Manuscript received July 4, 2012; revised August 30, 2012; accepted September 10, 2012. Date of publication September 28, 2012; date of current version October 31, 2012. This work was supported by the Hong Kong Government General Research Fund under Grant PolyU 5298/10E.

C. R. Liao and D. N. Wang are with the Department of Electrical Engineering, Hong Kong Polytechnic University, Hong Kong (e-mail: d.n.wang@polyu.edu.hk).

M. Wang and M. Yang are with the National Engineering Laboratory for Fiber Optic Sensing Technology, Wuhan University of Technology, Wuhan 430070, China.

Color versions of one or more of the figures in this letter are available online at http://ieeexplore.ieee.org.

Digital Object Identifier 10.1109/LPT.2012.2219517

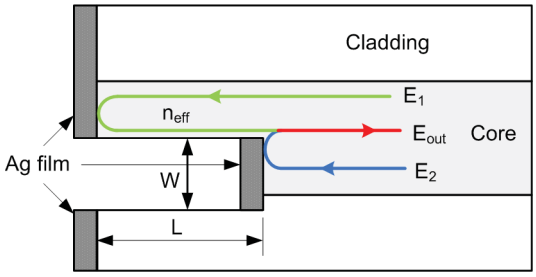

Fig. 1. Configuration of a fiber in-line MI.

II. Principle and Fabrication

A. Principle

Fig. 1 shows the schematic of the proposed MI. In a section of SMF, part of the fiber core near one fiber end is removed. Ag thin film is deposited on both the cut end of fiber core and the fiber end surfaces. The input light is split into two portions denoted by E_1 and E_2 respectively, with the splitting ratio of γ which depends on the width (W) of the cavity. After being reflected back by the fiber end, E_1 and E_2 are recombined at the cut end of the fiber core and results in interference. Assuming that the amplitude of the electrical field launched into the fiber is E_0, the output intensity of the MI is:

$$I_{out} = (E_0\gamma R\alpha)^2 + \left[E_0(1-\gamma)R\right]^2 + 2E_0^2R^2\gamma(1-\gamma)\alpha\cos(4\pi n_{eff}L/\lambda) \quad (1)$$

where R is the reflectivity at the end surfaces; α and n_{eff} are the propagation loss and the effective RI of the light propagating in the remaining fiber core, respectively, and L is the cavity length. When the phase term satisfies the condition $4\pi n_{eff}L/\lambda = (2m+1)\pi$, where m is an integer, an intensity minimum appears at the wavelength

$$\lambda_{dip} = 4n_{eff}L/(2m+1). \quad (2)$$

The fringe spacing and fringe visibility in the spectrum can then be expressed as

$$\Lambda \approx \lambda^2/2n_{eff}L \quad (3)$$

$$V = 2\alpha\cdot\left(\alpha^2\frac{\gamma}{1-\gamma}+\frac{1-\gamma}{\gamma}\right)^{-1}. \quad (4)$$

Eq. (4) indicates that the fringe visibility can be optimized by adjusting the splitting ratio which depends on cavity width.

B. Fabrication

Fig. 2 illustrates the fabrication process of the device. Fs laser pulses (800 nm, 120 fs, 1 kHz) were focused onto the fiber by an objective lens with NA value of 0.25. The pulse energy was adjustable between 0 and 1 mJ by an attenuator. A CCD camera was employed to monitor the fabrication process and record the sample morphology.

Firstly, the average on-target laser power was maintained at ~15 mW. A section of SMF was mounted on a translation stage. A broadband light source and an optical spectrum analyzer were employed to monitor the transmission spectrum in real-time. The laser beam was initially focused on the center of fiber core and then shifted by 15 μm away from the core axis. The rectangular cavity was created in SMF by fs laser ablation, in which the laser was scanned at a speed of 10 μm/s with the distance of 80 μm, in parallel with fiber axis. After each scanning cycle, the focal point of the laser beam was moved towards the core axis with a step of 1 μm before the next cycle started. The process continued until the expected transmission spectrum was obtained. By removing part of the fiber core near the core and cladding interface, an MZI structure was created [9] and the fringe visibility was optimized to be ~7 dB by controlling the diameter of the removed fiber core. The optical microscope image of the fiber MZI is shown in Fig. 2(a).

Secondly, the incident power was increased to 80 mW and the focal point of the laser beam was moved in perpendicular to the fiber axis with a speed of 100 μm/s, across the rectangular cavity. A micro-groove was created by such a laser scanning process in the middle of the cavity. The fiber sample was then cleaved by the local stress induced by the micro-groove and the corresponding optical microscope image is shown in Fig. 2(b).

Next, Ag thin film with a thickness of ~90 nm was coated on the fiber core and end surfaces by a BESTECH sputtering system. A 3-inch Ag target was installed and the distance between the fiber sample and target was ~150 mm. With a sputtering pressure of 0.5 Pa, the deposition power for Ag target was set as 100 W which corresponds to a deposition rate of ~0.2 nm/s. During the sputtering process, the thickness of Ag film was monitored by quartz crystal method.

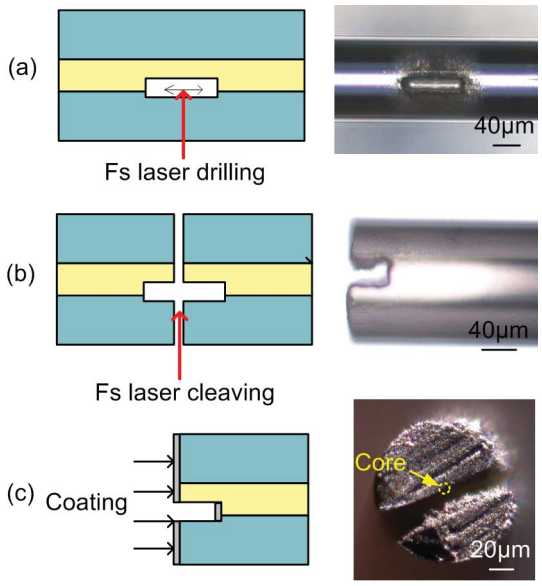

Fig. 2. Illustration of the fabrication process of the fiber in-line MI with optical microscope image taken at each stage. (a) Fs laser drilling of a rectangular cavity at the interface between the core and cladding. (b) Fs laser cleaving. (c) Ag film coating.

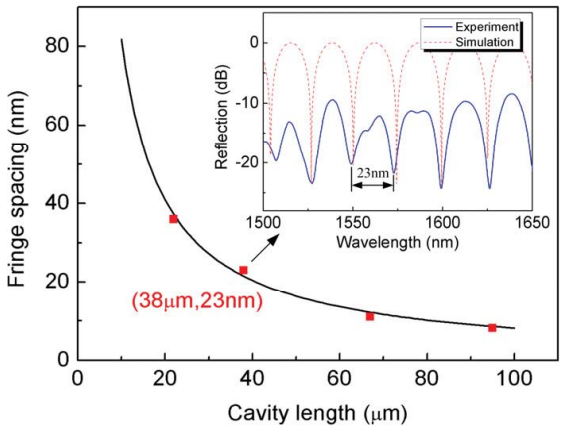

Fig. 3. Fringe spacing as a function of cavity length at the wavelength of ~1550 nm. The black line is the calculation result and the red square shows the experimentally obtained value. Inset: output spectrum of the fiber in-line MI with a cavity length of ~38 μm in experiment (blue line) and in simulation (red dotted line).

III. Results and Discussion

The output spectrum of the interferometer with cavity length of ~38 μm in air is shown in the inset of Fig. 3, where the red dotted line represents the calculated spectrum based on two-beam interferometry, which agrees well with the experimental results. The insertion loss of 10 dB mainly comes from the scattering at the cavity border and the reflection at Ag thin film. By optimizing the combination of the incident laser power and scanning speed, a smooth surface could be obtained, which helps in decreasing the scattering loss and enhancing the reflection of Ag film. The two exceptionally weak dips located at 1558 and 1586 nm may come from the multi-mode interference in the remaining fiber core. However, such a multi-mode interference does not play significant role in our experiment. The polarization dependent loss (PDL) was measured by a photonic all-parameter analyzer (Agilent 81910A), and a large PDL of 7 dB was obtained as the fs laser fabricated cavity introduces anisotropic features for waveguide beam.

By assuming $n_{eff} = 1.4682$, $\lambda = 1550$ nm, the fringe spacing variation with the cavity length were calculated according to Eq. (3), as shown in Fig. 3, where the black line stands for the calculated results and the red squares represent the experimentally obtained values. Only a small deviation is found, mainly due to the measurement error of the cavity length.

To experimentally study the relationship between the fringe visibility and the cavity size, the spectral evolution of our MI at different fabrication phases are displayed in Fig. 4. The black line shows the interference spectrum in phase1 (P1), with the cavity length of ~100 μm. In the next phase, P2, the cavity width is fixed and section A is removed, which increases

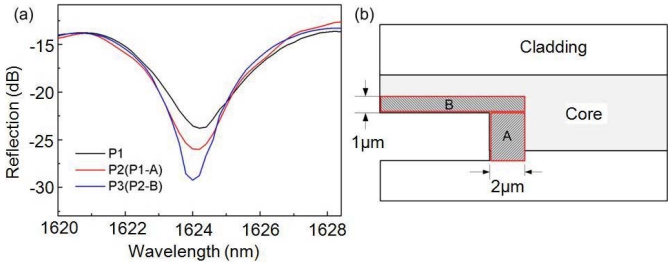

Fig. 4. (a) Spectral evolution of a fiber MI in different fabrication phases. (b) Schematic diagram of the fabrication.

the cavity length by ~2 μm and the spectrum obtained is shown by red line. Finally, section B is removed to increase the cavity width by ~1 μm and the spectrum in this phase (P3) is represented by the blue line. It can be found from Fig. 4 that the fringe visibility is determined by both the cavity width and cavity length, as explained by Eq. (4).

The output spectrum of the interferometer is critically dependent on the cavity length and the value of n_{eff}. The cavity length is a constant at a fixed temperature. The RI change of the ambient medium changes n_{eff} and results in a fringe dip shift. An experiment was implemented to test the RI response of the fiber in-line MI proposed. Room temperature was maintained in the experiment and the sensor head was sequentially immersed into a set of index matching oils (from Cargille Laboratory) ranging from 1.460 to 1.492 (@489.3 nm) with a step of 0.004. After each test, the device was carefully cleaned with isopropanol to remove the residual index oil and then dried in the air until the original spectrum was restored.

The output spectra of the interferometer exposed in air (blue line) and in the liquid with RI = 1.460 (red line) are shown in Fig. 5(a) for comparison. A significant fringe visibility reduction is observed which can be explained by the fact that the transmission loss is increased in the high-RI surrounding medium as less optical energy is confined in the remaining fiber core due to reduced RI difference between the core and the surrounding medium. The evolution of the two fringe dips around 1525 nm and 1630 nm are plotted in Fig. 5(b) and (c) respectively, with the RI changing from 1.460 to 1.488. The wavelength shifts of Dip 1 and Dip 2 with different RI values are displayed in Fig. 5(d), where the polynomial fit can be well implemented to the experimental data, denoted by black squares. With the increase of RI value, a nonlinear red shift appears for both the dips and hence a better sensitivity can be obtained in the high RI region. This phenomenon is widely existed in fiber evanescent-field RI sensors [4]. It is interesting to notice that the measurement range of the device is not limited by the fiber material, which overcomes the difficulty faced by fiber open-cavity FPI for RI sensing.

As shown in Fig. 5(d), Dip 2, positioned at a longer wavelength, exhibits a larger sensitivity to the ambient RI than that of Dip 1. The exact sensitivity value at each RI position can be obtained by calculating the first-order derivative of the wavelength shift. When RI = 1.484, the RI sensitivity is calculated to be 975 nm/RIU (refractive index unit) for Dip 2 and 463 nm/RIU for Dip 1, respectively. The machining accuracy

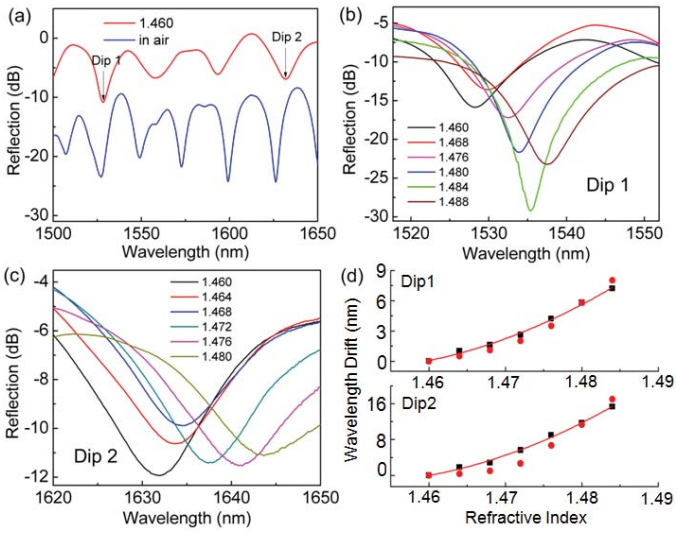

Fig. 5. (a) Reflection spectra of the fiber in-line MI tip sensor in air and in liquid with RI of 1.460. (b) Spectral evolution of fringe Dip 1 in different RI liquids. (c) Spectral evolution of fringe Dip 2 in different RI liquids. (d) Polynomial curve fitting of experimental data (black squares) showing the relationship between the wavelength shift of the fringe dip and the external RI value and simulation results (red circles).

of our fs laser system is ~1 μm and the converted sensing accuracy around 1550 nm is estimated to be ~1.3 nm/RIU.

For a constant cavity length, the RI sensitivity expression can be derived from Eq. (2) as,

$$\frac{d\lambda_{\text{dip}}}{dn} = \frac{4L}{2m+1} \cdot \frac{dn_{\text{eff}}}{dn} \tag{5}$$

where n denotes the RI of the ambient medium. It becomes clear from Eq. (5) that the sensitivity is dependent on n_{eff} which varies with the external RI. Considering the fundamental core mode, the mode energy profile at short wavelength would be mainly concentrated in the core, which leads that n_{eff} of the mode has only small sensitivity to the external RI variation. Further theoretical investigation for this was carried out by adopting a half-core model, with an FEM software package COMSOL. The calculated wavelength drifts of the two dips at ~1530 and ~1635 nm agree well with the experimental data as shown in Fig. 5(d).

By placing the fiber tip in an electrical oven and increasing the temperature from 20 to 90 °C with a step of 10 °C, a sensitivity of ~20 pm/°C was obtained. Based on the RI sensitivity of 975 nm/RIU, the temperature cross-sensitivity of the sensor is less than 2×10^{-5} RIU/°C.

Eq. (5) indicates that the sensitivity is directly proportional to the cavity length and hence an effective method to enhance the sensitivity is to increase the cavity length. However, the price paid is the increased insertion loss and decreased mechanical reliability due to dangling in air and gravity induced fiber bending which can be prevented by adopting a vertical tip sensor scheme. When immersing the fiber tip into liquid samples, the rough surface created by fs laser might make the existence of air bubbles. However, such air bubbles are too small to be observed and hence have no significant effect on our experimental results.

IV. Conclusion

In conclusion, a fiber in-line MI tip sensor based on open micro-cavity has been developed and used for RI sensing. The cavity is fabricated by fs laser micromachining with its end surfaces coated with Ag thin film to enhance the reflectivity. The RI sensitivity of the interferometer has been experimentally measured and analyzed and the results obtained show that the sensitivity is critically dependent on the selected operation wavelength and the cavity length, and a high sensitivity is associated with a large operation wavelength and a long cavity length. Such a fiber in-line interferometer exhibits the merits of compact size, good mechanical reliability, wide operation range and high sensitivity. Moreover, a reflection mode of detection is flexible and convenient in many sensing applications.

References

[1] C. E. Lee, H. F. Taylor, A. M. Markus, and E. Udd, "Optical-fiber Fabry–Pérot embedded sensor," *Opt. Lett.*, vol. 14, no. 21, pp. 1225–1227, Sep. 1989.

[2] J. Villatoro, V. Finazzi, G. Coviello, and V. Pruneri, "Photonic-crystal-fiber-enabled micro-Fabry–Pérot interfermoter," *Opt. Lett.*, vol. 34, no. 16, pp. 2441–2443, Aug. 2009.

[3] J. F. Ding, A. P. Zhang, L. Y. Shao, J. H. Yan, and S. L. He, "Fiber-taper seeded long period grating pair as a highly sensitive refractive-index sensor," *IEEE Photon. Technol. Lett.*, vol. 17, no. 6, pp. 1247–1249, Jun. 2005.

[4] Z. Tian, *et al.*, "Refractive index sensing with Mach–Zehnder interferometer based on concatenating two single-mode fiber tapers," *IEEE Photon. Technol. Lett.*, vol. 21, no. 8, pp. 161–163, Apr. 15, 2009.

[5] Z. B. Tian, S. S.-H. Yam, and H. P. Loock, "Single mode fiber refractive index sensor based on core-offset attenuators," *IEEE Photon. Technol. Lett.*, vol. 20, no. 16, pp. 1387–1389, Aug. 15, 2008.

[6] M. W. Yang, D. N. Wang, Y. Wang, and C. R. Liao, "Fiber in-line Mach–Zehnder interferometer constructed by selective infiltration of two air holes in photonic crystal fiber," *Opt. Lett.*, vol. 36, no. 5, pp. 636–638, Mar. 2011.

[7] Y. J. Rao, M. Deng, D. W. Duan, X. C. Yang, T. Zhu, and G. H. Cheng, "Micro Fabry–Pérot interferometers in silica fibers machined by femtosecond laser," *Opt. Express*, vol. 15, no. 21, pp. 14123–14128, Oct. 2007.

[8] J. L. Kou, J. Feng, L. Ye, F. Xu, and Y. Q. Lu, "Miniaturized fiber taper reflective interferometer for high temperature measurement," *Opt. Express*, vol. 18, no. 13, pp. 14245–14249, Jun. 2010.

[9] Y. Wang, M. W. Yang, D. N. Wang, S. Liu, and P. Lu, "Fiber in-line Mach–Zehnder interferometer fabricated by femtosecond laser micromachining for refractive index measurement with high sensitivity," *J. Opt. Soc. Amer. B*, vol. 27, no. 3, pp. 370–374, Mar. 2010.